Environmental Science & Technology

Article

Cite This: Environ. Sci. Technol. 2018, 52, 4040−4050

pubs.acs.org/est

Threshold Concentrations of Silver Ions Exist for the Sunlight-Induced Formation of Silver Nanoparticles in the Presence of Natural Organic Matter

Huiting Liu,[†] Xueyuan Gu,[†] Chenhui Wei,[†] Heyun Fu,[†] Pedro J.J. Alvarez,[§] Qilin Li,[§] Shourong Zheng,[†] Xiaolei Qu,*[,†] and Dongqiang Zhu[‡]

[†]State Key Laboratory of Pollution Control and Resource Reuse, School of the Environment, Nanjing University, Jiangsu 210023, China

[§]Department of Civil and Environmental Engineering, Rice University, Houston Texas 77005, United States

[‡]School of Urban and Environmental Sciences, Peking University, Beijing 100871, China

Supporting Information

ABSTRACT: Sunlight-induced photoformation of silver nanoparticles (nAg), mediated by natural organic matter (NOM), is significantly affected by the concentration of Ag(I) and chloride. The initial photoformation rates of nAg in Suwannee River humic acid (SRHA) and Suwannee River natural organic matter (SRNOM) solutions were examined under simulated sunlight irradiation. A critical induction concentration (CIC) of Ag(I) (10 mg/L for SRHA and 5 mg/L for SRNOM, respectively) was observed, below which the nAg formation was minimal. The threshold is attributed to the interplay of reduction and oxidation reactions mediated by NOM, reflecting the need to achieve sufficiently fast growth of silver clusters to outcompete oxidative dissolution. The CIC can be reduced by scavenging oxidative radicals or be increased by promoting singlet oxygen and hydrogen peroxide generation. The presence of chloride effectively reduced the CIC by forming AgCl, which facilitates reduction reactions and provides deposition surfaces. SRNOM is more efficient in mediating photoformation of nAg than SRHA, owing to their differed phototransient generation. These results highlight prerequisites for the photoformation of nAg mediated by NOM, in which the photochemistry and solution chemistry are both important.

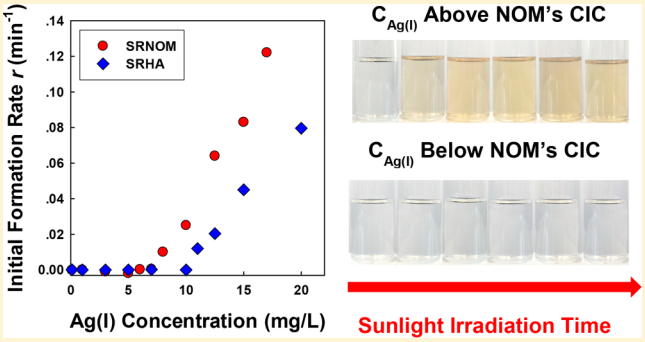

INTRODUCTION

Silver nanoparticles (nAg) possess unique optical, electronic, and antimicrobial properties and are the most widely used nanomaterial in consumer products.[1] When used as a strong and wide-spectrum antimicrobial agent, nAg can be readily incorporated into the matrix or the surface coating of textiles, personal-care products, medical devices, household appliances, and water treatment devices.[1] However, unintended nAg releases can adversely impact a wide range of organisms including microorganisms, algae, fungi, plants, invertebrates, vertebrates, and human cell lines.[2] The acute toxicity of nAg stems mainly from its ability to release Ag^+,[3,4] although nanoparticle-specific toxicity has also been reported.[5,6] The release of nAg/Ag^+ during the lifetime of these nano-enabled products seems inevitable and in many cases significant,[7,8] leading to concerns regarding its potential environmental risks.

The speciation of silver is critical for understanding the fate, bioavailability, and toxicity of nAg. It is well-known that nAg undergoes transformation processes including oxidation, dissolution, and reactions with ligands.[2] nAg can be oxidized by oxygen, forming a Ag_2O shell, which can subsequently release Ag^+.[9,10] Ag^+ can further complex with natural ligands, such as S^{2-}, Cl^-, and natural organic matter (NOM).[2,11] However, Ag^+ can be readily reduced by NOM to form new nAg under sunlight.[12−16] The photoreduction mechanism was suggested to be ligand-to-metal charge transfer (LMCT) and reduction mediated by phototransients such as superoxide (O_2^-).[14,15]

The impacts of water chemistry, including pH and coexisting cations, on the photoreduction process have been investigated.[12,14,15] Photoreduction rates increase with increasing pH,[12,14,15] owing to the pH-dependent Ag^+ sorption and reductive potential of NOM. The presence of coexisting cations reduced the formation rate of nAg, likely due to the competing effect for sorption sites on NOM.[14] Ca^{2+} was reported to induce the aggregation and formation of larger nAg particles.[12] Different NOM or NOM fractionations possess varying ability

Received: November 4, 2017
Revised: February 26, 2018
Accepted: March 5, 2018
Published: March 5, 2018

DOI: 10.1021/acs.est.7b05645
Environ. Sci. Technol. 2018, 52, 4040−4050

to photoreduce Ag^+, which can be attributed to the inherent reducing potential[16] and the differential light-attenuation ability.[12] Concurrent oxidation and dissolution and reduction reactions are previously reported to occur during the light-induced size and morphology evolution of nAg suspension.[13,14,17,18] In many cases, simulated sunlight was found to accelerate the dissolution of nAg through photo-oxidation processes.[13,19] However, little is known regarding how interactions between oxidative phototransients and silver species influence the initial photoformation of nAg in NOM solutions. Furthermore, little is known about the impact of chloride, which significantly influences silver speciation in aquatic environment, on the photoformation of nAg.

In the present study, we examine the sunlight-induced formation of nAg mediated by two standard humic substances, Suwannee River humic acid (SRHA) and Suwannee River natural organic matter (SRNOM), over a wide range of Ag(I) concentrations (0.05−20 mg/L). Our objectives were to (1) examine the possibility of forming nAg under more-realistic conditions found in sunlit natural aquatic systems and (2) elucidate the role of silver and chloride concentrations in the photoreduction process.

MATERIALS AND METHODS

Materials. Silver perchlorate (>97%), 2,3-bis (2-methoxy-4-nitro-5-sulfophenyl)-2H-tetrazolium-5-carboxanilide (XTT, > 90%), furfuryl alcohol (FFA, 98%), *N,N*-diethyl-p-phenylenediamine sulfate salt (DPD, ≥ 99%), horseradish peroxidase (HRP, ≥ 250 units/mg), and terephthalic acid (TPA, 98%) were purchased from Sigma-Aldrich. Deuteroxide (D_2O, 99.8 atom % D) was provided by Tokyo Chemical Industry. Isopropyl alcohol (>99.7%) was purchased from Nanjing Chemical Reagent Co., Ltd., China. All solutions were prepared using deionized water (18.2 MΩ·cm) obtained from an ELGA Labwater system (PURELAB Ultra, ELGA LabWater Global Operations).

Preparation of SRNOM and SRHA Solutions. NOM samples, including SRNOM and SRHA, were obtained from the International Humic Substances Society (IHSS, Saint Paul, MN). The stock solutions of NOM were prepared by dissolving 40 mg of sample powder into 100 mL of deionized water. It was then sonicated in a bath sonicator (KH-800TDB, Kunshan Hechuang Ultrasonic Instrument, China) at 50 W for 15 min. After adjustment of the pH to 7.0 ± 0.2 using 0.1 M NaOH, the NOM solutions were filtered through a 0.45 μm membrane (Pall). The total organic carbon (TOC) of NOM solutions was quantified by a TOC analyzer (TOC-5000A, Shimadzu). Part of the SRNOM solution was dialyzed using dialysis bags (1000 Da, Union Carbide) to remove the chloride.

Photoreduction of Ag^+. The photoreduction experiments were carried out by irradiating 30 mL of the Ag^+ and SRNOM or SRHA mixture stirred at 200 rpm in a 50 mL cylindrical cell equipped with a water-circulating jacket for temperature control. The concentration of Ag^+ (as $AgClO_4$) and Cl^- (as NaCl) stock solutions are 500 and 300 mg/L. A total of 1.08 mL of 139 mg C/L SRNOM stock solution or 0.69 mL of 217 mg C/L SRHA stock solution was mixed with predetermined amount of Ag^+ and Cl^- stock solutions to yield the experiment solution of 30 mL with total Cl^- concentration of 0.5 mg/L. The pH of the mixture was 7.0 ± 0.2 without buffer. The temperature of the circulating water was maintained at 20 ± 0.1 °C by a temperature control system (DC0506, Shanghai FangRui Instrument Co., Ltd.). The dissolved oxygen concentration in the test solution during the reaction remained constant at around 8 mg/L, as determined by an oxygen microsensor (PreSens, Precision Sensing GmbH; Figure S1). The simulated sunlight was provided by a 50 W xenon lamp (CEL-HXF300, AULTT) shining from the top of the cylindrical cell without light filters. The lamp spectrum was similar to that of natural sunlight with the wavelength of >300 nm (Figure S2). The irradiation energy at the water surface was 438 mW/cm^2, which was monitored periodically using a radiometer (CEL-NP2000−10, Ceaulight; Beijing, China). Samples were exposed to the same light intensity by adjusting the output energy to offset the decay of the lamp. The detailed experimental setup can be found in Figure S3. A small aliquot of 0.5 mL of solution was withdrawn periodically from the cell during the irradiation for analysis. Dark controls were conducted in the same experimental setting with the cell wrapped with aluminum foil and the xenon lamp off.

nAg Analysis. The formation of nAg was monitored by the absorbance of its surface plasmon resonance (SPR). UV−vis spectra of the samples were recorded using a double beam spectrophotometer (UV-6100, Mapada) in a quartz cell with 1 cm light path length. The detection limit for this method is around 0.01 mg/L nAg with diameter of 10 nm ±2 nm (Figure S4). The particle size of nAg was measured by dynamic light scattering (DLS) using a ZEN 3500 Zetasizer Nano ZS (Malvern) equipped with a 532 nm laser. In some experiments, the samples were concentrated by ultrafiltration membranes (Amicon Ultra-15 3 kDa, Millipore), dried on glass slides, and analyzed by an X-ray diffraction spectrometer (XRD, X-TRA, ALR).

ROS Determination. The production of $^1O_2$, $O_2^{\cdot-}$, H_2O_2, and ·OH and lower-energy hydroxylating species by SRNOM and SRHA was investigated using probe molecules as described previously.[20−25] $O_2^{\cdot-}$ generation was quantified by the formation of XTT formazan from XTT at an initial concentration of 0.05 mM. XTT formazan was quantified by its absorption at 470 nm. The extinction coefficient of XTT formazan is 23 800 M^{-1} cm^{-1}.[22] Singlet oxygen formation was monitored by the loss of FFA with an initial concentration of 0.05 mM.[26,27] The FFA concentration was measured at the detection wavelength of 220 nm using high-performance liquid chromatography (HPLC) with a Zorbax Eclipse XDB-C18 column (Agilent 1100, Agilent Technologies). The mobile phase was 30% acetonitrile and 70% 0.1 wt % phosphoric acid at a flow rate of 1 mL/min. The production of ·OH and lower-energy hydroxylating species was quantified by the loss of TPA.[23,25,28] TPA was added at a concentration of 0.5 mM into the NOM solutions. The residual TPA was quantified by HPLC using a mobile phase of 30% acetonitrile/70% 0.1 wt % phosphoric acid and a detection wavelength of 254 nm at a flow rate of 1 mL/min. H_2O_2 generation was measured by the HRP (5 mg/L) catalyzed oxidation of 1 mM DPD.[24] The stable oxidation product, $DPD^{\bullet+}$, was measured by its absorbance at 551 nm using a UV−vis spectrometer.

Batch-Sorption Experiments. Batch sorption experiments were conducted in 40 mL polypropylene centrifuge tubes filled with solutions containing 5 mg C/L SRNOM/SRHA and 0.1 to 20 mg/L Ag^+. The tubes were wrapped with aluminum foil and agitated on a reciprocating shaker at room temperature for 1 h, which was sufficient to achieve complexation equilibrium. A previous study suggested that the complexation between Ag^+ and NOM was almost instant (<1s).[29] The free Ag^+ was detected using a silver ion-selective electrode (9616BNWP,

DOI: 10.1021/acs.est.7b05645
Environ. Sci. Technol. 2018, 52, 4040−4050

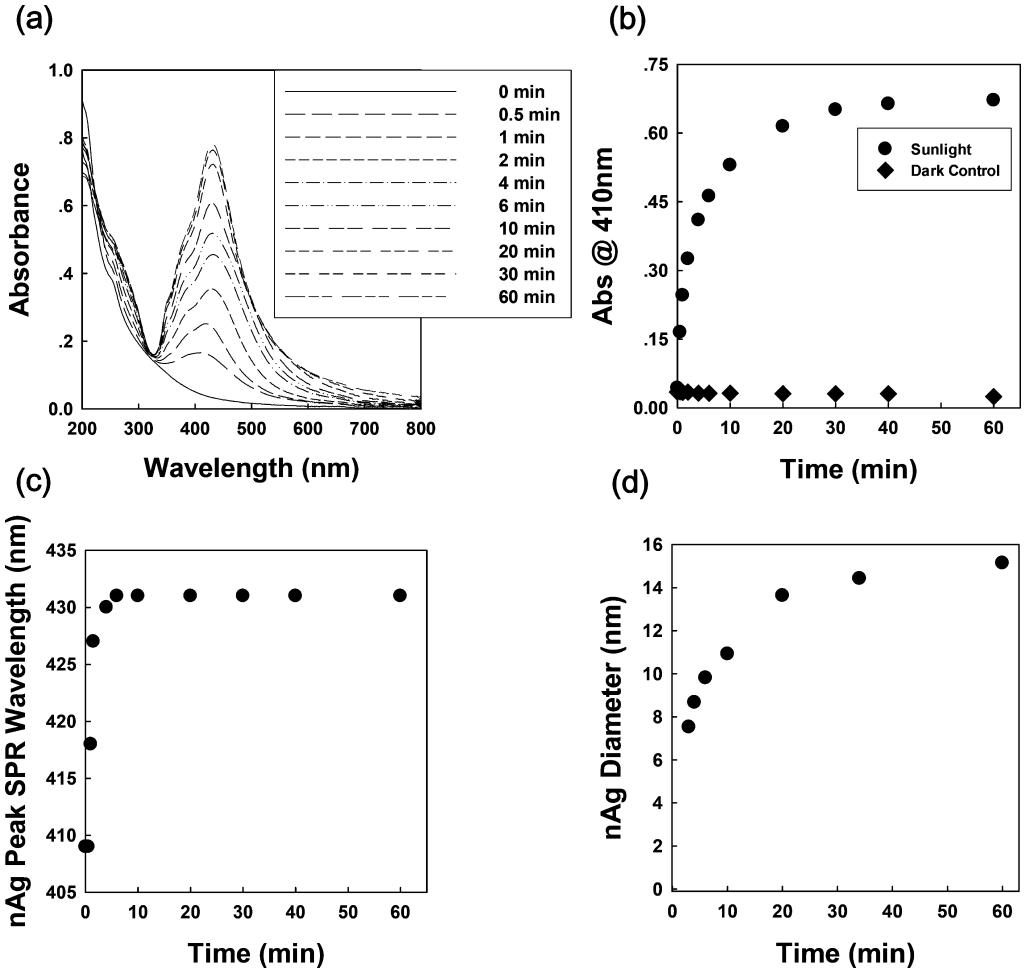

Figure 1. (a) UV−vis spectra of 20 mg/L Ag(I) and 5 mg C/L SRNOM during the simulated sunlight irradiation at pH 7.0 ± 0.2. (b) Formation kinetics of nAg during simulated sunlight irradiation and under dark condition in the presence of 20 mg/L Ag(I) and 5 mg C/L SRNOM, as quantified by the SPR absorbance at 410 nm. (c) Evolution of the SPR wavelength during the photoformation of nAg. (d) Particle diameter of nAg as a function of irradiation time as measured by dynamic light scattering.

Thermo) with a potentiometer (ORION 5 STAR, Thermo) at room temperature. The amount of AgCl formation was calculated by the loss of Cl^- in solution, which was determined using an ion chromatography (ICS-1000, Dionex) with a Dionex IonPac AS11-HC analytical column (250 mm × 4 mm). The mobile phase (1.0 mL/min) was 10 mM KOH. The concentrations of $AgCl_2^-$ and $AgCl_3^{2-}$ were several orders of magnitude lower than AgCl at experimental conditions and were consequently not considered in the mass balance.[30] The NOM-complexed Ag^+ at a specific equilibrium concentration was calculated based on the mass balance.

RESULTS AND DISCUSSION

Threshold Concentration of Ag(I) for the NOM-Mediated Photoformation of nAg. The UV−vis absorption spectra of the solution containing 20 mg/L Ag(I) and 5 mg C/L SRNOM during the simulated sunlight irradiation are shown in Figure 1a. The characteristic peak of the SPR of nAg at 409−431 nm was observed during the irradiation, which was consistent with previous photoreduction studies using humic substances.[14,16] An absorption minimum appeared at 320−334 nm; this was caused by the interband transition in nAg, which led to the damping of plasmon oscillations.[31] Figure 1b presents the formation kinetics of nAg under simulated sunlight exposure. The intensity of the SPR peak increased with longer irradiation time and plateaued after 40 min. Meanwhile, the wavelength of the SPR peak shifted from 409 to 431 nm in the initial 10 min, indicating the growth of nAg particle size upon simulated sunlight exposure (Figure 1c).[32,33] The wavelength of the SPR peak remained constant afterward, suggesting that the particle size plateaued. The DLS measurements showed a sharp increase of nAg size in 20 min, generally consistent with the initial shift of SPR peaks (Figure 1d). However, the particle size measured by DLS still increased after 20 min of irradiation. This could be attributed to morphology changes or the aggregation of nAg.[14,34]

To better understand the role of Ag(I) concentration and NOM properties in the photoreduction process, nAg formation kinetics were compared in the presence of SRNOM and SRHA. The initial formation rate of nAg, $r = (dA(t)/dt)_{t\to 0}$, was determined by linear regression of the initial increase of the SPR absorbance at 410 nm. The regression was carried out over 2 min of irradiation (see an example in Figure S5). The r has been reported to be proportional to the concentration of Ag(I) and NOM:[15]

$$r = k[\mathrm{Ag(I)}][\mathrm{NOM}] \quad (1)$$

DOI: 10.1021/acs.est.7b05645
Environ. Sci. Technol. 2018, 52, 4040−4050

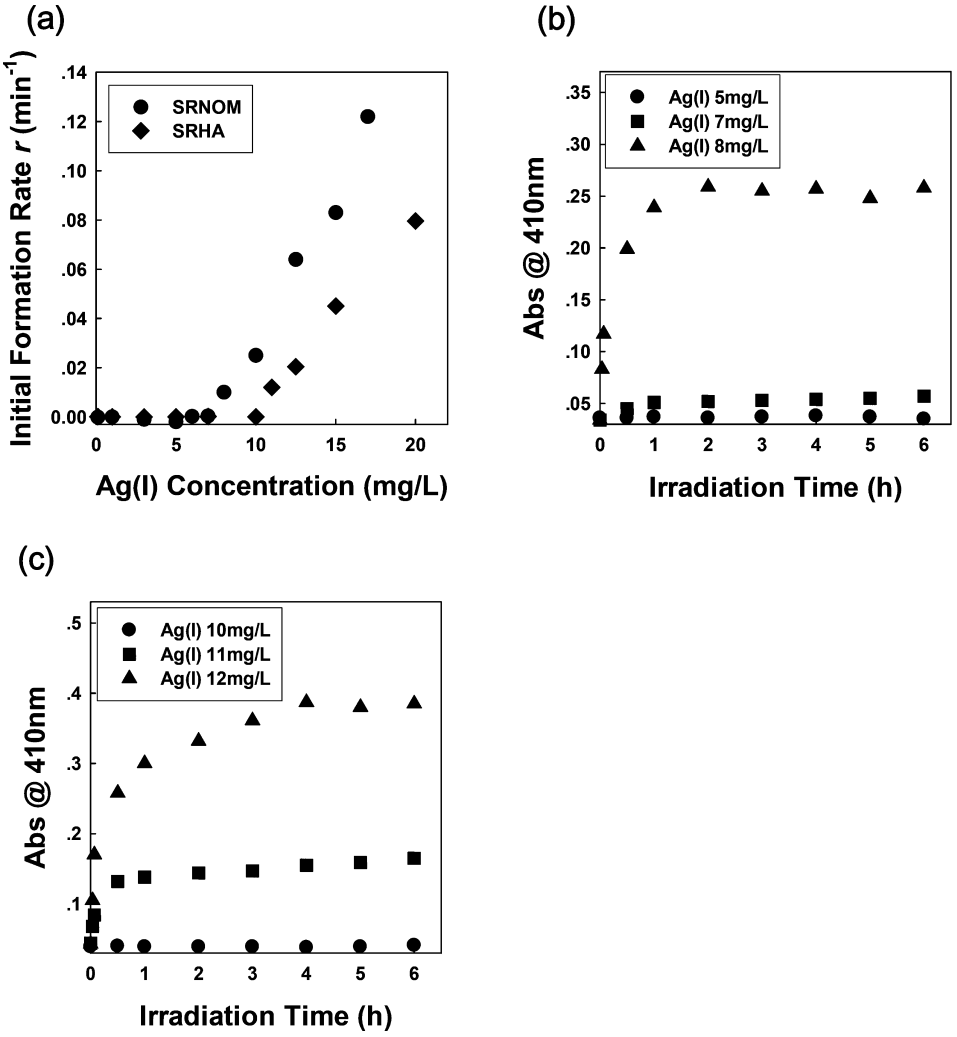

Figure 2. (a) Initial formation rate of nAg in 5 mg C/L SRNOM or SRHA solutions as a function of the Ag(I) concentration under simulated sunlight irradiation. Formation kinetics of nAg under simulated sunlight in the presence of 5 mg C/L (b) SRNOM and (c) SRHA at given concentrations of Ag(I) as quantified by the SPR absorbance at 410 nm. The solution pH was 7.0 ± 0.2, and the total chloride concentration was 0.5 mg/L.

Figure 2a shows the initial formation rate of nAg as a function of Ag(I) concentration in irradiated 5 mg C/L NOM solutions. It is worth noting that the Ag(I) concentration here refers to the total silver concentration including all silver species. Because the NOM concentration was set to be 5 mg C/L, r was expected to increase with increasing Ag(I) concentration according to eq 1. However, the profiles observed were composed of two distinct regimes: Regime I, at low Ag(I) concentration, in which no SPR absorbance of nAg was observed; and Regime II, once the Ag(I) concentration reached a threshold (referred to as critical induction concentration, CIC), in which r increased with increasing Ag(I) concentration. The CIC was 5 mg/L Ag(I) for SRNOM and 10 mg/L Ag(I) for SRHA, as suggested by the long-term irradiation tests (i.e., 6 h) (Figure 2b,c). It is worth noting that the CIC could be lower than what it appears to be in Figure 2a due to the extremely low initial formation rate near CIC, which can be determined in the long term irradiation tests. The CICs are much higher than the detection limit of the SPR method, 0.01 mg/L, and consequently can not be attributed to the detection method of nAg. The initial formation rate of nAg in NOM solutions decreased with decreasing light intensity (Figure S6a). Nevertheless, the CIC remained constant under simulated sunlight with different light intensities (Figure S6b).

The XRD pattern of the samples initially containing Ag(I) above CIC showed characteristic peaks for the (111), (200), and (220) planes of metallic silver (Figure 3b,d),[35] as well as a characteristic peak (2θ = 32.24°) for the (200) plane of AgCl. The total Cl^- concentration in the SRNOM and SRHA solutions was 0.5 mg/L, leading to the formation of AgCl (see the discussion about silver speciation below). The coexistence of metallic silver and AgCl during the photoformation of nAg mediated by riverine NOM was also reported in a previous study.[15] The characteristic peaks of metallic silver were found in the XRD pattern of the sample initially containing Ag(I) below CIC (i.e., no SPR observed) but with very low intensity (Figure 3a,c). Note that the detection limit of XRD is around 5%. The small amount of metallic silver detected could be attributed to the presence of dispersed Ag^0 or small silver clusters, which cannot induce SPR. Previous study suggested that noble metal clusters, such as Au clusters, with diameter smaller than 5 nm show little SPR but that show a sharp SPR with diameter of 5–50 nm.[36−38] According to the UV−vis and XRD data, the

DOI: 10.1021/acs.est.7b05645
Environ. Sci. Technol. 2018, 52, 4040−4050

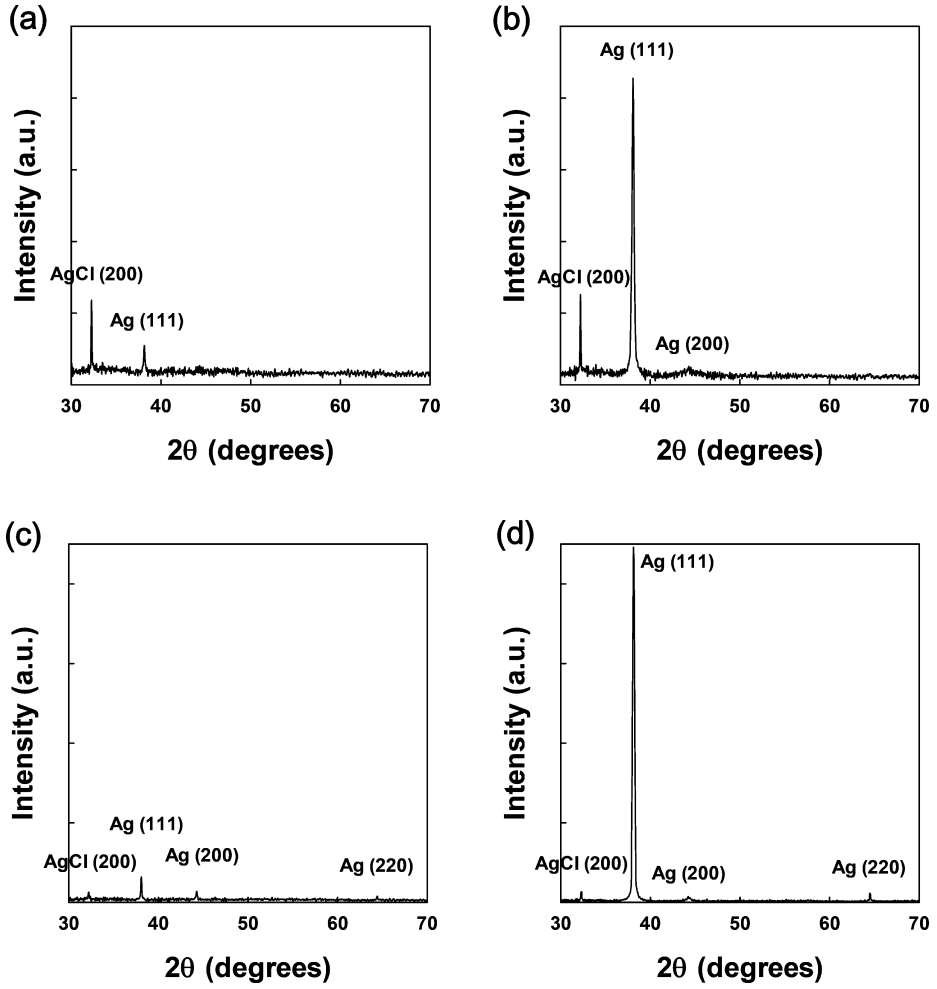

Figure 3. XRD spectra of samples containing (a) 3 mg/L Ag(I) (below CIC_{SRNOM}) and (b) 10 mg/L Ag(I) (above CIC_{SRNOM}) in 5 mg C/L SRNOM solutions; (c) 5 mg/L Ag(I) (below CIC_{SRHA}) and (d) 15 mg/L Ag(I) (above CIC_{SRHA}) in 5 mg C/L SRHA solutions after 30 min simulated sunlight irradiation. The solution pH was 7.0 ± 0.2, and the initial chloride concentration was 0.5 mg/L.

photoformation of nAg was minimal if not completely eliminated below CIC.

The concentrations of silver species including free Ag^+, NOM-complexed Ag^+, and AgCl in 5 mg C/L NOM solutions were summarized in Figure 4. The silver were mostly in the form of free Ag^+ and NOM-complexed Ag^+. Over the entire Ag(I) concentration tested, free Ag^+ constituted 20−75% of total silver in SRNOM solution and 21−68% of total silver in SRHA solution. NOM-complexed Ag^+ constituted 20−73% of total silver in SRNOM solution and 26−67% of total silver in SRHA solution. The AgCl formed at low Ag^+ concentrations due to its small solubility product, 1.77×10^{-10}.[2] Its concentration stabled after the majority of chloride in the system was scavenged. The speciation diagram suggests that the CIC was not caused by the precipitation of Ag^+ as AgCl.

Interplay of Reduction and Oxidation Reactions Affected the CIC. The observation of a minimum threshold concentration, CIC, implies the presence of antagonistic reactions to the photoreductive formation of nAg. We hypothesize that this can be attributed to the interplay of reduction and oxidation reactions between phototransients and silver species, which control the nucleation and growth of silver clusters. Concurrent oxidation and dissolution and reduction reactions are previously reported to occur during the light-induced size and morphology evolution of nAg suspension.[13,14,17,18] In many cases, simulated sunlight was found to accelerate the dissolution of nAg through photo-oxidation processes.[13,19]

NOM can reduce Ag^+ to silver atoms (Ag^0) under simulated sunlight irradiation through two possible pathways: (1) direct transfer of electrons to complexed Ag^+ through the LMCT pathway or (2) generation of O_2^-, which, in turn, reduces Ag^+ (eqs 2 and 3):[14,15,39]

$$Ag^+ + e^- \rightarrow Ag^0 \quad (2)$$

$$Ag^+ + O_2^- \rightarrow Ag^0 + O_2 \quad (3)$$

$$Ag^0 + Ag^0 \rightarrow Ag^0_2 \quad (4)$$

Ag^0 forms dimers when it collides:[40]

$$Ag_m + Ag_n \rightarrow Ag_{m+n} \quad (5)$$

Further coalescence results in silver clusters and, eventually, nAg particles.[41]

Under solar irradiation, SRNOM and SRHA can be excited, generating singlet excited state NOM (^{1}NOM*) and charge-separated species ($NOM^{\pm}$).[42] $NOM^{\pm}$ can react with the complexed Ag^+ through the LMCT pathway. ^{1}NOM* further undergo energy-transfer or charge-transfer reactions to form various phototransients including $NOM^{\pm}$, O_2^-, $^1O_2$, H_2O_2, and

DOI: 10.1021/acs.est.7b05645
Environ. Sci. Technol. 2018, 52, 4040−4050

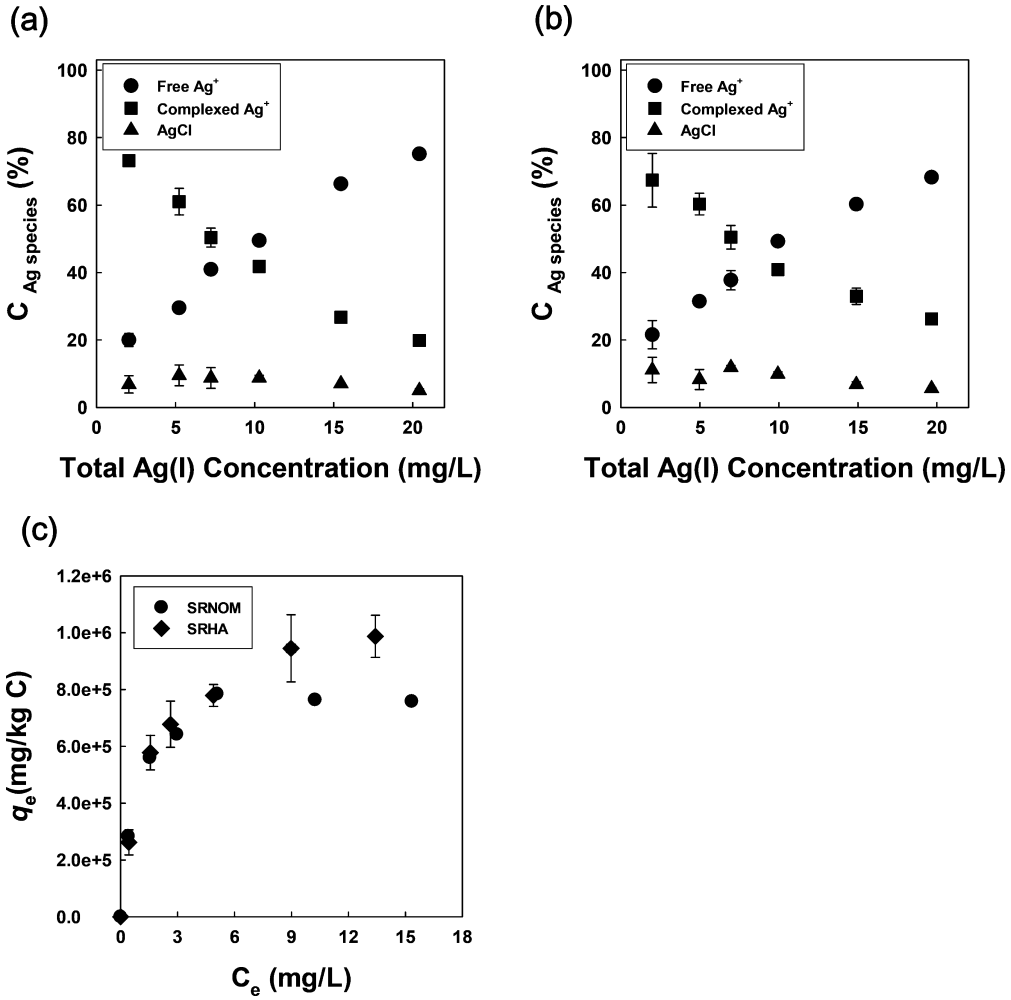

Figure 4. Speciation of silver in 5 mg C/L (a) SRNOM and (b) SRHA solutions plotted as percentages of silver species vs the initial total Ag(I) concentration; (c) sorption isotherms plotted as complexed concentration (q_e, mg/kg C) vs aqueous-phase concentration (C_e, mg/L) of Ag^+ at equilibrium in the presence of 5 mg C/L SRNOM or SRHA at pH 7.0 ± 0.2. The total chloride concentration was 0.5 mg/L. Sorption experiments were run in triplicate.

·OH and lower-energy hydroxylating species, which are expected to mediate the redox reactions of silver species.[42,43] The O_2^- generation in SRNOM and SRHA solutions was quantified and compared in Figure 5a. A recent study suggested that the XTT assay was not specific to O_2^- in some cases.[44] Nevertheless, the reduction of XTT was almost completely inhibited in the presence of 15 mg/L superoxide dismutase (Figure S7), confirming the generation of O_2^-.[44] The rate of O_2^- generation in the SRNOM solution was higher than that in the SRHA solution (Figure 5a). Other than reductive O_2^-, SRHA and SRNOM are known to generate oxidative ROS, including $^1O_2$, H_2O_2, and ·OH and lower-energy hydroxylating species under solar irradiation,[45,46] which are compared in panels b–d of Figure 5, respectively. SRNOM produced similar amount of $^1O_2$ as compared to SRHA (Figure 5b). The apparent singlet oxygen quantum yields of SRNOM and SRHA were calculated to be 1.60% and 1.16% (see details in the Supporting Information), respectively, generally consistent with previous reported values (i.e., 2.02 ± 0.23% and 1.81% for SRNOM and 1.38 ± 0.08% and 1.60 ± 0.08% for SRHA).[20,45,47] SRNOM generated less H_2O_2 and ·OH and lower-energy hydroxylating species than did SRHA (Figure 5c,d). The lower ·OH and lower-energy hydroxylating species generation rate of SRNOM agrees with a previous report.[25] The oxidizing species, including $^1O_2$, H_2O_2, and ·OH and lower-energy hydroxylating species can readily oxidize Ag^0 or nAg at neutral pH.[10,17,48−51] The steady-state concentration of $^1O_2$ and ·OH and lower-energy hydroxylating species in 5 mg C/L SRNOM solution are calculated to be 3.2×10^{-13} and 1.3×10^{-16} M, respectively (see details in the Supporting Information). If we assume a diffusion-limited reaction constant between Ag^0 and these phototransients ($k = 1 \times 10^{10}$ M^{-1} s^{-1}),[39] the reaction rate constants are 3.2×10^{-3} s^{-1} and 1.6×10^{-6} s^{-1} for $^1O_2$ and ·OH and lower-energy hydroxylating species, respectively. It is worth noting that there is strong microheterogeneity of phototransients in irradiated NOM solutions.[52] For example, the $^1O_2$ in NOM microenvironment, $[^1O_2]_{NOM}$, is much higher than $[^1O_2]$ measured by FFA method. The reactions between Ag^0 and $^1O_2$ happened mostly in NOM. If we use the $[^1O_2]_{NOM}/[^1O_2]$ of 130 from the literature,[52] the reaction rate constant between Ag^0 and $^1O_2$ can be as high as 0.42 s^{-1}. This indicates that Ag^0 can potentially be oxidized by phototransients generated by NOM within a short time scale. Previous studies suggested that the interactions between these oxidizing species and citrate-coated/bare nAg facilitated their photoinduced dissolution process.[17,53] SRNOM

DOI: 10.1021/acs.est.7b05645
Environ. Sci. Technol. 2018, 52, 4040−4050

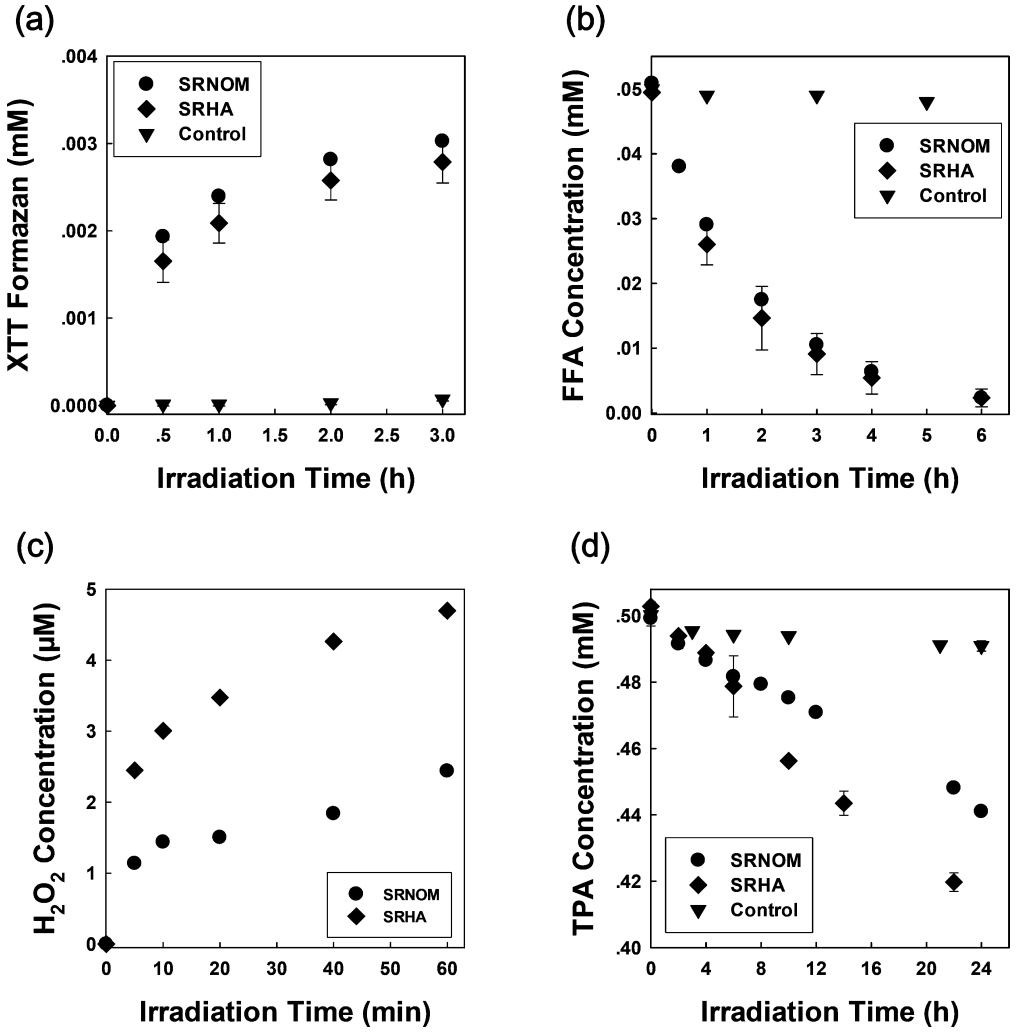

Figure 5. (a) XTT formazan production, representing O_2^- generation; (b) FFA degradation, representing $^1O_2$ generation; (c) H_2O_2 generation; and (d) TPA degradation, representing •OH generation as a function of irradiation time with 26.8 mg C/L NOM under simulated sunlight. Error bars represent plus or minus one standard deviation from the average of triplicate tests.

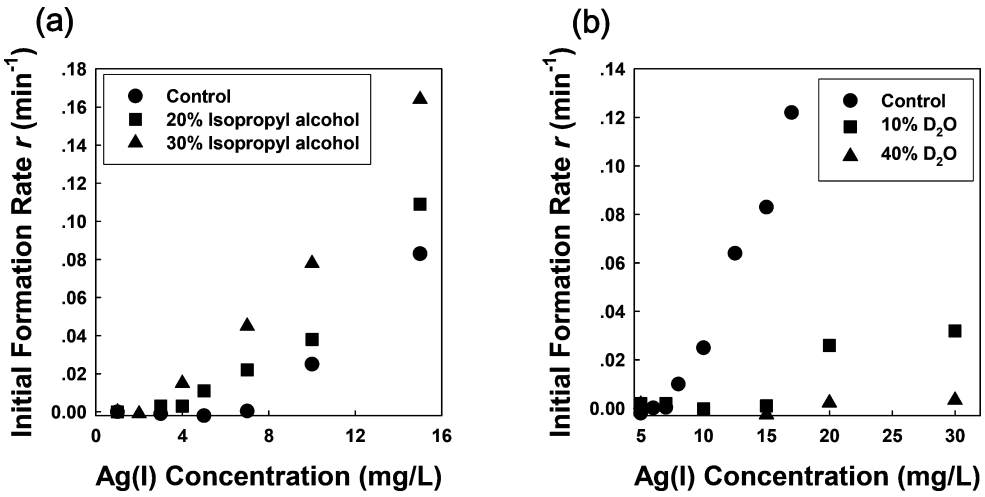

Figure 6. Initial formation rate of nAg in 5 mg C/L SRNOM solutions as a function of the Ag(I) concentration in the presence of (a) isopropyl alcohol and (b) D_2O under simulated sunlight irradiation. The solution pH was 7.0 ± 0.2, and the initial chloride concentration was 0.5 mg/L.

generated more reductive O_2^-, a similar amount of $^1O_2$, but less H_2O_2 and ·OH and lower-energy hydroxylating species than SRHA, consistent with its lower CIC (i.e., NOM with higher O_2^- generation and lower $^1O_2$, H_2O_2, ·OH, and lower-energy hydroxylating species generation possesses lower CIC value).

DOI: 10.1021/acs.est.7b05645
Environ. Sci. Technol. 2018, 52, 4040−4050

To further probe the interplay of oxidation and reduction reactions in the photoformation of nAg, we carried out scavenger tests. Isopropyl alcohol was first introduced into the reaction system as a radical scavenger, especially for ·OH and lower-energy hydroxylating species.[54,55] The CIC of SRNOM decreased from 5 to 2 mg/L as the concentration of isopropyl alcohol increased from 0 to 30%, as shown in Figure 6a. It suggests that the CIC_{SRNOM} can be lowered by scavenging oxidative radicals in the system. Another test was carried out in the presence of D_2O as shown in Figure 6b. The presence of D_2O had no impact on the measurement of nAg SPR (Figure S8). D_2O can promote the lifetime of $^1O_2$ (16-fold greater than in H_2O solution)[56] and consequently increase its steady-state concentration. This is caused by the kinetic solvent isotope effect as the $^1O_2$ deactivation rate constant is much lower in D_2O than that in H_2O.[56] Meanwhile, the H_2O_2 generation rate by SRNOM was also expected to increase in the presence of D_2O.[57] The CIC_{SRNOM} was found to increase from 5 to 15 mg/L as the concentration of D_2O increased from 0 to 10% (Figure 6b). In the presence of 40% D_2O, the nAg formation kinetics was low even at 30 mg/L Ag(I). These results suggest that the CIC can be manipulated by scavenging or promoting the oxidative phototransients, indicating that the CIC can be at least partially attributed to the balance between redox reactions.

As the Ag(I) concentration exceeded CIC, nAg started to form. This indicates that the balance between redox reactions can be modulated by the Ag(I) concentration. We speculate that higher Ag(I) concentration facilitates the nucleation and growth of silver clusters. The presence and growth of silver clusters can facilitate the photoreduction process by increasing the redox potential of Ag^+ and inducing the catalytic reduction of Ag^+.[39,58−60] Free Ag^+ in solutions has a redox potential of −1.8 V ($Ag^+ + e^- \rightarrow Ag^0$; $E^0 = -1.8$ V versus NHE).[59] Thus, silver atoms are not stable compared to the Ag^+/e^- couple. In the presence of silver clusters, Ag^+ was mainly reduced on the cluster surface. The redox potential of Ag^+ increases with increasing coexisting silver cluster size and eventually reaches +0.8 V in the presence of nAg particles.[60,61] Silver clusters were suggested to rapidly store and transfer electrons to oxygen or Ag^+, catalyzing the reduction reactions of Ag^+.[39,58] It has been reported that the presence of nAg led to 4 times faster Ag^+ reduction by O_2^-.[39] However, the growth of silver clusters hindered the oxidation process as larger silver clusters are more resistant to oxidation and subsequent dissolution due to its higher redox potentials and lower specific surface area.[2,62,63] We speculate that higher Ag(I) concentration can facilitate the initial nucleation and growth of silver clusters by increasing the kinetics of coalescence among Ag^0 (eq 4) or small silver clusters (eq 5). It may also promote the kinetics of surface Ag^+ reduction on silver clusters, which leads to their growth. Once the Ag(I) concentration exceeds the CIC, silver clusters undergo fast coalescence and surface Ag^+ reduction, which helps them grow to a critical size at which reduction outcompetes oxidation and subsequent dissolution.

At low silver concentrations, a significant part of silver will be complexed with NOM. An earlier study suggests that the photoreduction process involves Ag^+ binding to NOM.[14] Thus, the initial formation of silver clusters can be affected by the complexed Ag^+ concentration in NOM molecules. The complexed Ag^+ concentration was much higher than that in the bulk solution depending on the complexation affinity of NOM. The carbon-normalized Ag^+ complexation affinities of SRNOM and SRHA were compared in Figure 4c. SRHA had stronger complexation affinity than SRNOM at high silver concentrations, consistent with a previous study on the Ag^+-NOM interactions.[29] Their complexation affinities were similar at low silver concentrations. At the Ag(I) concentrations of 5 mg/L (CIC_{SRNOM}) and 10 mg/L (CIC_{SRHA}), the complexed Ag^+ concentrations in SRNOM and SRHA were similar. Thus, the differed CIC of SRNOM and SRHA was not caused by the different complexed Ag^+ concentration in NOM. The higher ability of SRNOM in mediating the photoformation of nAg is most likely due to its higher reductive phototransient generation but lower oxidative phototransient generation.

Impact of Chloride on the CIC. Chloride is ubiquitous in natural aquatic systems and is known to strongly influence the speciation of silver and the dissolution of nAg.[18] To test the role of Cl^- in the photoformation of nAg, nAg formation kinetics in SRNOM solution was determined at various Cl^- concentrations as shown in Figure 7. The CIC_{SRNOM} was found to decrease with increasing Cl^- concentration. It decreased from 10 to 3 mg/L as the Cl^- concentration increased from 0.23 to 1 mg/L. In another experiment, we used dialysis method to remove the Cl^- ion from the SRNOM solution (data labeled as 0 mg/L Cl^- in Figure 7). There was no nAg formation in the dialyzed SRNOM solution at silver concentration of 20 mg/L. Note that part of the low-molecular-weight fraction of SRNOM (~15%) was removed during dialysis. A previous study suggested that all size fractions of SRNOM were photoactive and the difference of size fractions on the photoreduction of silver was caused by the differential light attenuation.[12] Thus, the inhibited nAg formation in the dialyzed SRNOM solution was attributed to the removal of Cl^- rather than the removal of low-molecular-weight fraction of SRNOM.

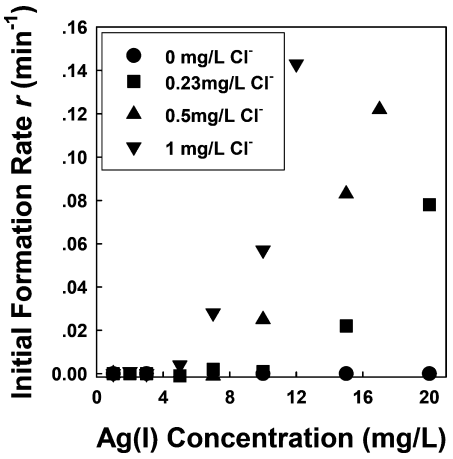

Figure 7. Initial formation rate of nAg in 5 mg C/L SRNOM solutions as a function of the Ag(I) concentration at various chloride concentrations under simulated sunlight irradiation. The solution pH was 7.0 ± 0.2.

AgCl is a semiconductor photocatalyst that generates electron−hole pairs under simulated sunlight.[64] The electron transfer can reduce Ag^+ at the surface of AgCl, which produces Ag^0 atoms that potentially combine with adjacent atoms to yield silver clusters or nAg.[30,64] Furthermore, on irradiation, AgCl itself can partially transform into nAg.[65,66] This process is often used to prepare Ag@AgCl photocatalyst.[64] A recent study also suggested that an important role of AgCl in the

DOI: 10.1021/acs.est.7b05645
Environ. Sci. Technol. 2018, 52, 4040−4050

photoreduction of Ag^+ in the presence of peptides was to provide deposition surfaces.[67] However, The coexisting AgCl is also known to generate various oxidizing species including holes, chlorine atoms, ·OH, hydrogen peroxide, and carbonate radicals.[68] The formation of AgCl also decreased the total amount of free and NOM-complexed Ag^+. Our results suggest that the overall effect of AgCl in the tested conditions is to facilitate the photoformation of nAg. Nevertheless, the presence of AgCl does not necessarily lead to the formation of nAg through aforementioned mechanisms in our systems (Figure 4a,b). This result indicates that photoformation of nAg is still controlled by the redox balance after taking the role of AgCl into consideration.

Environmental Implications. Our work demonstrates the existence of a threshold concentration of Ag^+ for the photoformation of nAg mediated by NOM. The CIC is defined by the photochemistry of NOM and is influenced by the water chemistry. The CIC of NOM in natural conditions could be lower than the CIC values of SRNOM and SRHA, which are both in the milligram per liter range. However, the Ag^+ concentration in natural surface waters is in the range of nanograms to micrograms per liter,[69,70] several orders of magnitude lower than the CIC determined in our experimental settings. The growth of silver clusters is expected to be slow due to the extremely low mass transfer at environmental concentrations, which may not be sufficiently fast to outcompete oxidative dissolution. Thus, the possibility of NOM-mediated photoformation of nAg in natural aquatic conditions needs to be further scrutinized. The existence of a threshold also indicates that some of the results acquired using high Ag^+ concentrations cannot be linearly extrapolated to environmental conditions. The photoformation of nAg could be potentially relevant for surface waters heavily impacted by silver input, such as wastewater effluents or mine drainage with comparatively high silver concentrations. In that case, the most-abundant silver species is often silver sulfide, which can be transformed into nAg by photoinduced Fe redox cycling.[71] In another possible scenario, the photoformation of nAg could be triggered by pre-existing silver seeds. Silver clusters can be generated from the reduction of Ag^+ in the presence of microbes, extracellular polymeric substances, or humic substances under natural conditions without light exposure,[16,72−74] serving as seeds for faster photoreduction reactions.

■ ASSOCIATED CONTENT

Supporting Information

The Supporting Information is available free of charge on the ACS Publications website at DOI: 10.1021/acs.est.7b05645.

Figures showing dissolved oxygen concentration in the test solution during the irradiation, the spectra of the xenon lamp and sunlight, the experimental setup for irradiation experiments, UV−vis spectra, the initial formation rates of nAg, and XTT formazan production. Details on the calculation of the apparent quantum yield of singlet oxygen. (PDF)

■ AUTHOR INFORMATION

Corresponding Author

*Phone: +86-025-8968-0256; e-mail: xiaoleiqu@nju.edu.cn.

ORCID

Xueyuan Gu: 0000-0002-8521-3667

Qilin Li: 0000-0001-5756-3873

Shourong Zheng: 0000-0001-8660-4910

Xiaolei Qu: 0000-0002-9157-4274

Dongqiang Zhu: 0000-0001-6190-5522

Notes

The authors declare no competing financial interest.

■ ACKNOWLEDGMENTS

We thank Ziyan Du, Zhixian Li, Yutong Xu, and Yufan Li for their assistance in measuring nAg photoformation kinetics. This work was supported by the National Key Basic Research Program of China (grant no. 2014CB441103), the National Natural Science Foundation of China (grant nos. 21407073, 21622703, 21225729, and 21237002), and the Department of Science and Technology of Jiangsu Province (grant no. BE2015708). We thank the State Key Laboratory of Environmental Chemistry and Ecotoxicology, Research Center for Eco-Environmental Sciences, Chinese Academy of Sciences for partial funding (KF2014-11). Partial funding was also provided by the NSF ERC on Nanotechnology-Enabled Water Treatment (grant no. EEC-1449500).

■ REFERENCES

(1) The Project on Emerging Nanotechnologies. Nanotechnology Home Page, Consumer Products Inventory. http://www.nanotechproject.org/cpi/ (accessed on August 20th, 2015).

(2) Levard, C.; Hotze, E. M.; Lowry, G. V.; Brown, G. E. Environmental transformations of silver nanoparticles: Impact on stability and toxicity. *Environ. Sci. Technol.* **2012**, *46*, 6900−6914.

(3) Xiu, Z. M.; Zhang, Q. B.; Puppala, H. L.; Colvin, V. L.; Alvarez, P. J. J. Negligible particle-specific antibacterial activity of silver nanoparticles. *Nano Lett.* **2012**, *12*, 4271−4275.

(4) Xiu, Z. M.; Ma, J.; Alvarez, P. J. J. Differential effect of common ligands and molecular oxygen on antimicrobial activity of silver nanoparticles versus silver ions. *Environ. Sci. Technol.* **2011**, *45*, 9003−9008.

(5) Fabrega, J.; Fawcett, S. R.; Renshaw, J. C.; Lead, J. R. Silver nanoparticle impact on bacterial growth: Effect of pH, concentration, and organic matter. *Environ. Sci. Technol.* **2009**, *43*, 7285−7290.

(6) Yin, L.; Cheng, Y.; Espinasse, B.; Colman, B. P.; Auffan, M.; Wiesner, M.; Rose, J.; Liu, J.; Bernhardt, E. S. More than the ions: The effects of silver nanoparticles on Lolium multiflorum. *Environ. Sci. Technol.* **2011**, *45*, 2360−2367.

(7) Benn, T. M.; Westerhoff, P. Nanoparticle silver released into water from commercially available sock fabrics. *Environ. Sci. Technol.* **2008**, *42*, 4133−4139.

(8) Benn, T.; Cavanagh, B.; Hristovski, K.; Posner, J. D.; Westerhoff, P. The release of nanosilver from consumer products used in the home. *J. Environ. Qual.* **2010**, *39*, 1875−1882.

(9) Cai, W.; Zhong, H.; Zhang, L. Optical measurements of oxidation behavior of silver nanometer particle within pores of silica host. *J. Appl. Phys.* **1998**, *83*, 1705−1710.

(10) Liu, J.; Hurt, R. H. Ion release kinetics and particle persistence in aqueous nano-silver colloids. *Environ. Sci. Technol.* **2010**, *44*, 2169−2175.

(11) Lowry, G. V.; Espinasse, B. P.; Badireddy, A. R.; Richardson, C. J.; Reinsch, B. C.; Bryant, L. D.; Bone, A. J.; Deonarine, A.; Chae, S.; Therezien, M.; Colman, B. P.; Hsu-Kim, H.; Bernhardt, E. S.; Matson, C. W.; Wiesner, M. R. Long-term transformation and fate of manufactured Ag nanoparticles in a simulated large scale freshwater emergent wetland. *Environ. Sci. Technol.* **2012**, *46*, 7027−7036.

(12) Yin, Y. G.; Shen, M. H.; Zhou, X. X.; Yu, S. J.; Chao, J. B.; Liu, J. F.; Jiang, G. B. Photoreduction and stabilization capability of molecular weight fractionated natural organic matter in transformation of silver ion to metallic nanoparticle. *Environ. Sci. Technol.* **2014**, *48*, 9366−9373.

DOI: 10.1021/acs.est.7b05645
Environ. Sci. Technol. 2018, 52, 4040−4050

(13) Yu, S. J.; Yin, Y. G.; Chao, J. B.; Shen, M. H.; Liu, J. F. Highly dynamic PVP-coated silver nanoparticles in aquatic environments: Chemical and morphology change induced by oxidation of Ag^0 and reduction of Ag^+. *Environ. Sci. Technol.* **2014**, *48*, 403−411.
(14) Hou, W. C.; Stuart, B.; Howes, R.; Zepp, R. G. Sunlight-driven reduction of silver ions by natural organic matter: Formation and transformation of silver nanoparticles. *Environ. Sci. Technol.* **2013**, *47*, 7713−7721.
(15) Yin, Y. G.; Liu, J. F.; Jiang, G. B. Sunlight-induced reduction of ionic Ag and Au to metallic nanoparticles by dissolved organic matter. *ACS Nano* **2012**, *6*, 7910−7919.
(16) Adegboyega, N. F.; Sharma, V. K.; Siskova, K.; Zboril, R.; Sohn, M.; Schultz, B. J.; Banerjee, S. Interactions of aqueous Ag^+ with fulvic acids: Mechanisms of silver nanoparticle formation and investigation of stability. *Environ. Sci. Technol.* **2013**, *47*, 757−764.
(17) Li, Y.; Niu, J.; Shang, E.; Crittenden, J. Photochemical transformation and photoinduced toxicity reduction of silver nanoparticles in the presence of perfluorocarboxylic acids under UV irradiation. *Environ. Sci. Technol.* **2014**, *48*, 4946−4953.
(18) Zhou, W.; Liu, Y. L.; Stallworth, A. M.; Ye, C.; Lenhart, J. J. Effects of pH, electrolyte, humic acid, and light exposure on the long-term fate of silver nanoparticles. *Environ. Sci. Technol.* **2016**, *50*, 12214−12224.
(19) Grillet, N.; Manchon, D.; Cottancin, E.; Bertorelle, F.; Bonnet, C.; Broyer, M.; Lermé, J.; Pellarin, M. Photo-oxidation of individual silver nanoparticles: A real-time tracking of optical and morphological changes. *J. Phys. Chem. C* **2013**, *117*, 2274−2282.
(20) Dalrymple, R. M.; Carfagno, A. K.; Sharpless, C. M. Correlations between dissolved organic matter optical properties and quantum yields of singlet oxygen and hydrogen peroxide. *Environ. Sci. Technol.* **2010**, *44*, 5824−5829.
(21) Chen, C. Y.; Jafvert, C. T. The role of surface functionalization in the solar light-induced production of reactive oxygen species by single-walled carbon nanotubes in water. *Carbon* **2011**, *49*, 5099−5106.
(22) Sutherland, M. W.; Learmonth, B. A. The tetrazolium dyes MTS and XTT provide new quantitative assays for superoxide and superoxide dismutase. *Free Radical Res.* **1997**, *27*, 283−289.
(23) Fu, H. Y.; Liu, H. T.; Mao, J. D.; Chu, W. Y.; Li, Q. L.; Alvarez, P. J. J.; Qu, X. L.; Zhu, D. Q. Photochemistry of dissolved black carbon released from biochar: Reactive oxygen species generation and phototransformation. *Environ. Sci. Technol.* **2016**, *50*, 1218−1226.
(24) Hsieh, H. S.; Wu, R. R.; Jafvert, C. T. Light-independent reactive oxygen species (ROS) formation through electron transfer from carboxylated single-walled carbon nanotubes in water. *Environ. Sci. Technol.* **2014**, *48*, 11330−11336.
(25) Page, S. E.; Arnold, W. A.; McNeill, K. Assessing the contribution of free hydroxyl radical in organic matter-sensitized photohydroxylation reactions. *Environ. Sci. Technol.* **2011**, *45*, 2818−2825.
(26) Haag, W. R.; Hoigne, J.; Gassman, E.; Braun, A. M. Singlet oxygen in surface waters. 1. Furfuryl alcohol as a trapping agent. *Chemosphere* **1984**, *13*, 631−640.
(27) Qu, X. L.; Alvarez, P. J. J.; Li, Q. L. Photochemical transformation of carboxylated multiwalled carbon nanotubes: Role of reactive oxygen species. *Environ. Sci. Technol.* **2013**, *47*, 14080−14088.
(28) Page, S. E.; Arnold, W. A.; McNeill, K. Terephthalate as a probe for photochemically generated hydroxyl radical. *J. Environ. Monit.* **2010**, *12*, 1658−1665.
(29) Mousavi, M. P. S.; Gunsolus, I. L.; Pérez De Jesús, C. E.; Lancaster, M.; Hussein, K.; Haynes, C. L.; Bühlmann, P. Dynamic silver speciation as studied with fluorous-phase ion-selective electrodes: Effect of natural organic matter on the toxicity and speciation of silver. *Sci. Total Environ.* **2015**, *537*, 453−461.
(30) Liu, J.; Sonshine, D. A.; Shervani, S.; Hurt, R. H. Controlled release of biologically active silver from nanosilver surfaces. *ACS Nano* **2010**, *4*, 6903−6913.
(31) Evanoff, D. D.; Chumanov, G. Size-controlled synthesis of nanoparticles. 1. "Silver-only" aqueous suspensions via hydrogen reduction. *J. Phys. Chem. B* **2004**, *108*, 13948−13956.
(32) Peng, S.; McMahon, J. M.; Schatz, G. C.; Gray, S. K.; Sun, Y. G. Reversing the size-dependence of surface plasmon resonances. *Proc. Natl. Acad. Sci. U. S. A.* **2010**, *107*, 14530−14534.
(33) Kelly, K. L.; Coronado, E.; Zhao, L. L.; Schatz, G. C. The optical properties of metal nanoparticles: The influence of size, shape, and dielectric environment. *J. Phys. Chem. B* **2003**, *107*, 668−677.
(34) Li, X.; Lenhart, J. J. Aggregation and dissolution of silver nanoparticles in natural surface water. *Environ. Sci. Technol.* **2012**, *46*, 5378−5386.
(35) Sun, Y.; Xia, Y. Shape-controlled synthesis of gold and silver nanoparticles. *Science* **2002**, *298*, 2176−2179.
(36) Henglein, A.; Meisel, D. Radiolytic control of the size of colloidal gold nanoparticles. *Langmuir* **1998**, *14*, 7392−7396.
(37) Henglein, A. Radiolytic preparation of ultrafine colloidal gold particles in aqueous solution: Optical spectrum, controlled growth, and some chemical reactions. *Langmuir* **1999**, *15*, 6738−6744.
(38) Kamat, P. V. Photophysical, photochemical and photocatalytic aspects of metal nanoparticles. *J. Phys. Chem. B* **2002**, *106*, 7729−7744.
(39) Jones, A. M.; Garg, S.; He, D.; Pham, A. N.; Waite, T. D. Superoxide-mediated formation and charging of silver nanoparticles. *Environ. Sci. Technol.* **2011**, *45*, 1428−1434.
(40) Ershov, B. G.; Janata, E.; Henglein, A.; Fojtik, A. Silver atoms and clusters in aqueous solution: Absorption spectra and the particle growth in the absence of stabilizing Ag^+ ions. *J. Phys. Chem.* **1993**, *97*, 4589−4594.
(41) Belloni, J. Nucleation, growth and properties of nanoclusters studied by radiation chemistry: Application to catalysis. *Catal. Today* **2006**, *113*, 141−156.
(42) Sharpless, C. M.; Blough, N. V. The importance of charge-transfer interactions in determining chromophoric dissolved organic matter (CDOM) optical and photochemical properties. *Environ. Sci.-Process Impacts* **2014**, *16*, 654−671.
(43) McNeill, K.; Canonica, S. Triplet state dissolved organic matter in aquatic photochemistry: Reaction mechanisms, substrate scope, and photophysical properties. *Environ. Sci.-Process Impacts* **2016**, *18*, 1381−1399.
(44) Zhao, J. F.; Zhang, B. W.; Li, J. Y.; Liu, Y. C.; Wang, W. F. Photo-enhanced oxidizability of tetrazolium salts and its impact on superoxide assaying. *Chem. Commun.* **2016**, *52*, 11595−11598.
(45) Zhang, D. N.; Yan, S. W.; Song, W. H. Photochemically induced formation of reactive oxygen species (ROS) from effluent organic matter. *Environ. Sci. Technol.* **2014**, *48*, 12645−12653.
(46) Zhou, H.; Lian, L.; Yan, S.; Song, W. Insights into the photo-induced formation of reactive intermediates from effluent organic matter: The role of chemical constituents. *Water Res.* **2017**, *112*, 120−128.
(47) Mostafa, S.; Rosario-Ortiz, F. L. Singlet oxygen formation from wastewater organic matter. *Environ. Sci. Technol.* **2013**, *47*, 8179−8186.
(48) Graedel, T. E. Corrosion mechanisms for silver exposed to the atmosphere. *J. Electrochem. Soc.* **1992**, *139*, 1963−1970.
(49) Geranio, L.; Heuberger, M.; Nowack, B. The behavior of silver nanotextiles during washing. *Environ. Sci. Technol.* **2009**, *43*, 8113−8118.
(50) He, D.; Garg, S.; Waite, T. D. H_2O_2-mediated oxidation of zero-valent silver and resultant interactions among silver nanoparticles, silver ions, and reactive oxygen species. *Langmuir* **2012**, *28*, 10266−10275.
(51) He, D.; Jones, A. M.; Garg, S.; Pham, A. N.; Waite, T. D. Silver nanoparticle−reactive oxygen species interactions: Application of a charging−discharging model. *J. Phys. Chem. C* **2011**, *115*, 5461−5468.
(52) Latch, D. E.; McNeill, K. Microheterogeneity of singlet oxygen distributions in irradiated humic acid solutions. *Science* **2006**, *311*, 1743−1747.
(53) Zhang, W.; Li, Y.; Niu, J. F.; Chen, Y. S. Photogeneration of reactive oxygen species on uncoated silver, gold, nickel, and silicon

DOI: 10.1021/acs.est.7b05645
Environ. Sci. Technol. 2018, 52, 4040−4050

nanoparticles and their antibacterial effects. *Langmuir* **2013**, *29*, 4647−4651.
(54) Luo, N.; Kombo, D. C.; Osman, R. Theoretical studies of hydrogen abstraction from 2-propanol by OH radical. *J. Phys. Chem. A* **1997**, *101*, 926−936.
(55) Ryan, C. C.; Tan, D. T.; Arnold, W. A. Direct and indirect photolysis of sulfamethoxazole and trimethoprim in wastewater treatment plant effluent. *Water Res.* **2011**, *45*, 1280−1286.
(56) Wilkinson, F.; Helman, W. P.; Ross, A. B. Rate constants for the decay and reactions of the lowest electronically excited singlet-state of molecular-oxygen in solution: An expanded and revised compilation. *J. Phys. Chem. Ref. Data* **1995**, *24*, 663−1021.
(57) Garg, S.; Rose, A. L.; Waite, T. D. Photochemical production of superoxide and hydrogen peroxide from natural organic matter. *Geochim. Cosmochim. Acta* **2011**, *75*, 4310−4320.
(58) Henglein, A.; Lilie, J. Storage of electrons in aqueous-solution: The rates of chemical charging and discharging the colloidal silver microelectrode. *J. Am. Chem. Soc.* **1981**, *103*, 1059−1066.
(59) Linnert, T.; Mulvaney, P.; Henglein, A.; Weller, H. Long-lived nonmetallic silver clusters in aqueous solution: Preparation and photolysis. *J. Am. Chem. Soc.* **1990**, *112*, 4657−4664.
(60) Gentry, S. T.; Fredericks, S. J.; Krchnavek, R. Controlled particle growth of silver sols through the use of hydroquinone as a selective reducing agent. *Langmuir* **2009**, *25*, 2613−2621.
(61) Henglein, A. Small-particle research: Physicochemical properties of extremely small colloidal metal and semiconductor particles. *Chem. Rev.* **1989**, *89*, 1861−1873.
(62) Ivanova, O. S.; Zamborini, F. P. Size-dependent electrochemical oxidation of silver nanoparticles. *J. Am. Chem. Soc.* **2010**, *132*, 70−72.
(63) Henglein, A. Physicochemical properties of small metal particles in solution: "Microelectrode" reactions, chemisorption, composite metal particles, and the atom-to-metal transition. *J. Phys. Chem.* **1993**, *97*, 5457−5471.
(64) Wang, P.; Huang, B. B.; Qin, X. Y.; Zhang, X. Y.; Dai, Y.; Wei, J. Y.; Whangbo, M. H. Ag@AgCl: A highly efficient and stable photocatalyst active under visible light. *Angew. Chem., Int. Ed.* **2008**, *47*, 7931−7933.
(65) Garg, S.; Ma, T.; Miller, C. J.; Waite, T. D. Mechanistic insights into free chlorine and reactive oxygen species production on irradiation of semiconducting silver chloride particles. *J. Phys. Chem. C* **2014**, *118*, 26659−26670.
(66) Yin, Y.; Xu, W.; Tan, Z.; Li, Y.; Wang, W.; Guo, X.; Yu, S.; Liu, J.; Jiang, G. Photo- and thermo-chemical transformation of AgCl and Ag_2S in environmental matrices and its implication. *Environ. Pollut.* **2017**, *220*, 955−962.
(67) Kracht, S.; Messerer, M.; Lang, M.; Eckhardt, S.; Lauz, M.; Grobety, B.; Fromm, K. M.; Giese, B. Electron transfer in peptides: On the formation of silver nanoparticles. *Angew. Chem., Int. Ed.* **2015**, *54*, 2912−2916.
(68) Ma, T.; Garg, S.; Miller, C. J.; Waite, T. D. Contaminant degradation by irradiated semiconducting silver chloride particles: Kinetics and modelling. *J. Colloid Interface Sci.* **2015**, *446*, 366−372.
(69) Ndung'u, K.; Ranville, M. A.; Franks, R. P.; Flegal, A. R. On-line determination of silver in natural waters by inductively-coupled plasma mass spectrometry: Influence of organic matter. *Mar. Chem.* **2006**, *98*, 109−120.
(70) Rivera-Duarte, I.; Flegal, A. R. Pore-water silver concentration gradients and benthic fluxes from contaminated sediments of San Francisco Bay, California, U.S.A. *Mar. Chem.* **1997**, *56*, 15−26.
(71) Li, L.; Zhou, Q.; Geng, F.; Wang, Y.; Jiang, G. Formation of nanosilver from silver sulfide nanoparticles in natural waters by photoinduced Fe(II, III) redox cycling. *Environ. Sci. Technol.* **2016**, *50*, 13342−13350.
(72) Akaighe, N.; MacCuspie, R. I.; Navarro, D. A.; Aga, D. S.; Banerjee, S.; Sohn, M.; Sharma, V. K. Humic acid-induced silver nanoparticle formation under environmentally relevant conditions. *Environ. Sci. Technol.* **2011**, *45*, 3895−3901.
(73) Adegboyega, N. F.; Sharma, V. K.; Siskova, K. M.; Vecerova, R.; Kolar, M.; Zboril, R.; Gardea-Torresdey, J. L. Enhanced formation of silver nanoparticles in Ag^+-NOM-Iron(II, III) systems and antibacterial activity studies. *Environ. Sci. Technol.* **2014**, *48*, 3228−3235.
(74) Kang, F. X.; Alvarez, P. J. J.; Zhu, D. Q. Microbial extracellular polymeric substances reduce Ag^+ to silver nanoparticles and antagonize bactericidal activity. *Environ. Sci. Technol.* **2014**, *48*, 316−322.

DOI: 10.1021/acs.est.7b05645
Environ. Sci. Technol. 2018, 52, 4040−4050